Chemical Engineering Journal 530 (2026) 173630

Contents lists available at ScienceDirect

Chemical Engineering Journal

journal homepage: www.elsevier.com/locate/cej

Effect of reactor configuration of surface dielectric barrier discharge in contact with liquids on the production of reactive species

Oleksandr Galmiz *, Richard Cimerman, Zdenko Machala

Division of Environmental Physics, Faculty of Mathematics, Physics and Informatics, Comenius University in Bratislava, Mlynská dolina, 842 48, Bratislava, Slovakia

ARTICLE INFO

Keywords:
SDBD
Plasma
Liquid electrodes
RONS
Reactor

ABSTRACT

Surface dielectric barrier discharge (SDBD), ignited directly from liquid electrodes at the three-phase plasma/liquid/solid interface, represents a novel approach to liquid and polymer surface treatment. This study examines the formation of reactive oxygen and nitrogen species (RONS) in both gas and liquid phases, focusing on the effects of reactor geometry and electrode liquid type—oxalic acid solution and tap water were tested. Ozone dominated the gas phase in the open-air reactor, whereas restricting the air volume above the discharge increased the relative humidity and the concentration of nitrogen-containing species. The spatial limitations of the discharge region also affected the pH of the treated liquid. In the liquid phase, key RONS (H_2O_2, NO_2^-, NO_3^-, O_3) were identified. The liquid type had the most pronounced effect on NO_2^- and NO_3^- formation dynamics. The concentrations of all detected species increased with the plasma energy density input. Additionally, electrical measurements of the SDBD with liquid electrodes were performed, and its operational characteristics are discussed. While various reactor configurations may be used in practice, our results demonstrate that the choice of setup significantly influences the underlying plasma chemistry and must be carefully considered in real-world applications.

1. Introduction

Electrical discharges in contact with liquids, and especially water, have captured the attention of scientists and engineers worldwide in recent years [1] due to their remarkable potential for a diverse range of applications, including decontamination [2,3], nanoparticle synthesis [4,5], ozone generation [6,7], plasma medicine [8], and food processing [9]. Among these applications, surface activation of various materials stands out as a particularly compelling area of research due to their inherent high reactivity and adaptability to a wide range of materials [10].

Dielectric barrier discharges (DBDs) have evolved as one of the most widely employed techniques for material surface activation using atmospheric-pressure plasmas. For over half a century, DBDs have been instrumental in modifying and functionalizing the surface properties of synthetic polymers and other materials [11,12].

When treating sensitive polymer samples, however, the higher-density plasma can cause the so-called pin-holing effect and lead to undesired damage to the sensitive material surface integrity. This is a problem of volume barrier discharges or coronas, where the plasma discharge filaments propagate perpendicular to the treated surface. One of the options to overcome this negative effect is to generate plasma discharges that propagate in parallel with the sample. One of the basic configurations of DBDs is the surface dielectric barrier discharge (SDBD) arrangement, where the discharge develops along the dielectric surface owing to the tangential electric field introduced by aptly positioned metallic electrodes on opposite faces of the dielectric. This not only maintains the material integrity but also enhances the overall effectiveness of the plasma treatment.

Discharges generated in contact with water or other liquids represent a unique class of non-thermal atmospheric pressure plasma sources, due to their ability to produce strongly oxidizing species and UV radiation [13]. The resulting plasma-activated liquids (PAL) contain various reactive oxygen and nitrogen species (RONS) and exhibit potential benefits for chemical and biological applications [14]. PAL chemical properties and effects strongly depend on the plasma sources and discharge regimes used, and their interaction with water [15].

Moreover, the interface between the plasma and liquid and solid phases plays a very important role in PAL formation [16,17].

In conventional SDBD systems, the plasma is typically confined to a

* Corresponding author.
E-mail address: oleksandr.galmiz@uniba.sk (O. Galmiz).

https://doi.org/10.1016/j.cej.2026.173630
Received 22 September 2025; Received in revised form 14 December 2025; Accepted 29 January 2026
Available online 30 January 2026

thin layer that forms along the surface of the dielectric barrier, without direct contact with the liquid phase. While this configuration is effective for generating a wide range of reactive species in the gas phase, it presents a notable limitation when applied to water treatment. Specifically, the lack of direct plasma-liquid interaction severely restricts the transfer of short-lived, highly oxidative radicals into the aqueous phase. The configuration used in this study overcomes previous limitations by employing liquids as electrodes, enabling the plasma ignition directly from the liquid surface.

By relocating the discharge region from a remote dielectric surface to the liquid boundary itself, this approach significantly enhances the transfer and immediate utilization of short-lived reactive species within the aqueous environment. Furthermore, by adjusting the liquid level or repositioning the dielectric, the plasma region can be guided along the entire length of the tubular object, enabling continuous and uniform treatment of hollow objects like pipes, tubes, and catheters. This approach enables to attain a highly oxidative plasma without succumbing to the issues of electrode erosion. Moreover, this unique approach offers additional capabilities, such as rapid plasma-assisted liquid functionalization, providing a one-step process compared to traditional wet chemistry.

This study introduces a method that harnesses the benefits of water discharges and SDBD by utilizing a water solution as a discharge electrode. The key innovation lies in manipulating the height of the liquid level surrounding the dielectric body (e.g., polymer tubes) and the liquid that fills it. This allows precise control over the plasma ignition location at the three-phase (plasma-liquid-solid) interface, inside or outside the dielectric body.

Building upon the foundation established in our prior research [18–22], where we successfully developed and demonstrated a novel plasma discharge reactor capable of efficiently activating polymeric materials at the gas/liquid interface, the present study seeks to advance this work by exploring the underlying chemical dynamics in greater depth. Specifically, we aim to elucidate the composition and evolution of reactive chemical species in both the liquid and gas phases during the operation of an SDBD system configured with liquid electrodes.

To this end, we investigate three distinct reactor configurations incorporating liquid electrodes, enabling a comparative analysis of how structural and operational parameters influence the plasma-induced chemistry. A central goal of this study is to deepen the understanding of physicochemical interactions at the plasma–liquid boundary, particularly the mechanisms governing the formation and transformation of reactive species that are critical to plasma-assisted polymer modification and broader surface engineering applications.

Understanding the interplay between the discharge characteristics, the reactor geometry, and the chemical outcomes is essential for the rational design and optimization of plasma-based processes. We demonstrate that variations in parameters—including power input, electrode configuration, and liquid composition—can significantly affect the nature and abundance of reactive species, and hence the overall efficacy of the treatment. Furthermore, altering the liquid composition affects the chemical environment in which the plasma-generated species react, thereby influencing the resulting product distribution. This effect is relevant for applications in plasma-assisted material modification and functionalization, where the reaction outcomes are critical. This work addresses the knowledge gaps by revealing how the reactor geometry, confinement, and the chosen liquid jointly determine gas-phase chemistry and liquid-phase RONS formation, enabling more controlled and application-oriented plasma–liquid processes.

2. Experimental setup and techniques employed

2.1. Experimental setup

To simulate the gas/liquid/dielectric interface (i.e., the three-phase interface) under stable conditions, a thin glass test tube with an outer diameter of 10 mm and a wall thickness of 0.5 mm filled with conductive liquid was employed. During the experiments, two types of liquids were used as high-voltage liquid electrodes. The first liquid was a 5%wt solution of oxalic acid dihydrate (approx. 7 g of $(COOH)_2{\cdot}2H_2O$ per 100 ml) diluted by deionized water. This solution is stable over time, and its electrical conductivity does not change much even when reused in the following experiments. The choice of oxalic acid instead of some inorganic solutions was made to prevent the formation of inorganic salt crystals. We have found that the formation of salt crystals on discharge dielectrics markedly deteriorates the discharge uniformity. Thanks to the high electrical conductivity of its water solutions, oxalic acid represents an ideal electrolytic salt. In all experiments, the conductivity of the solution was 4.75 mS cm^{-1}. This solution was used in our previous works and proved to be efficient from the perspective of material processing [20,23,24]. The same oxalic acid solution was always used as a second electrode (not in contact with the plasma) in all reactors.

The potential impact of oxalic acid on gas-phase analysis was carefully considered. It is known that when oxalic acid vapor is heated (typically between 400 and 430 K), it can decompose into formic acid (HCOOH) and carbon dioxide (CO_2), with smaller amounts of other products such as carbon monoxide (CO) and water (H_2O) under specific conditions, including photolysis. Matrix effects of oxalic acid on RONS concentrations were evaluated using reference samples. No measurable influence was observed for RONS determinations.

The second type of liquid was tap water. It is a commonly available, simple liquid medium with a conductivity of ~400 μS/cm that is enough to transfer the discharge electric current.

Since for each specific industrial application, the configuration of the plasma reactor could be different, three different experimental reactors were tested. Fig. 1 displays the schematic arrangements of the plasma reactors along with their photographs. *"Open"* reactor corresponds to the configuration when the outer side of the polymer tube is treated (Fig. 1 (a, b)). The ambient air surrounding the plasma region is not limited in any way. The liquid inside the test tube was connected to the high-voltage power supply, generating a sine voltage waveform. The liquid in the Petri dish was grounded. Both electrically insulated solutions (inside and outside the test tube) served as liquid electrodes.

The *"Closed"* reactor is identical to the *"Open"* reactor, the only difference is that the reactor chamber was closed by the lid (Fig. 1 (c, d)). By doing this, we can collect all the species that were produced during the discharge operation, and the limited gas volume (30 ml) resulted in higher gas temperatures and humidity.

In the case of *"Open"* and *"Closed"* reactors, the liquid level inside the tube was always higher than in the surrounding bath. As a consequence, the SDBD was generated on the outer surface of the test glass tube and initiated from the waterline of the outer liquid electrode. To keep the same electrical parameters (discharge frequency, conductive current values) for the cases of *"Open"* and *"Closed"* reactors, the level of tube immersion was kept the same (7 mm). The volume of the treated liquid was 10 ml. The maximum treatment time was 15 min.

On the contrary, in the case of the *"In tube"* reactor, the surrounding liquid level was higher than in the test tube, which promoted the ignition of plasma inside the tube (Fig. 1 (e, f)). Because of the limited gas volume inside the tube (5 ml), it is expected that the gas temperature and its humidity will change during the plasma operation, hence, the amounts of the produced species. The SDBD reactor temperature (plasma, gas, and surface) depends on the injection and dynamic dissipation of energy in time and space, and it affects the chemical reaction rates, background gas density, and reactive species transport properties, which determine the discharge chemistry, electrical parameters, and, consequently, the generation of reactive species [25]. During the plasma treatment within the *"In tube"* reactor, we had to limit the liquid volume to 1 ml (due to the tube dimensions). Thus, the treatment time was capped at a maximum of 3 min. The distance between the metal electrodes was kept at 2.5 cm for all three reactors.

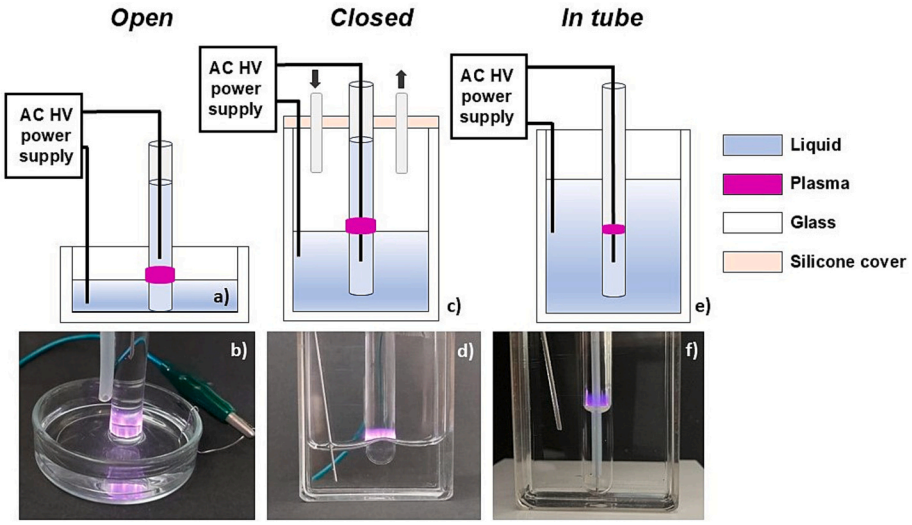

Fig. 1. Schematic arrangement and photo of the *"Open"* (a, b), *"Closed"* (c, d), and *"In tube"* (e, f) plasma reactors.

The discharge was operated in the ambient air at atmospheric pressure. The experimental setup is presented in Fig. 2. The high-voltage sine waveform was set to an amplitude of 6 to 13 kV (depending on the applied power) and operated at the adjustable frequency in the range of 26–31 kHz. For comparison, Table 1 presents the parameters for different reactors at 10 W discharge power. The power to the liquid electrodes was supplied by a high-voltage resonance generator (*Lifetech-300 W*) coupled with a function generator (*FY3200S-24 M*). The electrical characteristics of the discharge were monitored by a digital oscilloscope (*Tektronix TBS 2104*; 100 MHz; 1 GSa/s) connected to voltage (*Tektronix P6015A*) and current (*Pearson Electronics 4100*) probes. The Lissajous figure method, displaying the applied voltage and the transferred charge, was used to calculate the discharge power. The standard deviation of the measured power was estimated to be a maximum of 0.5 W. The additional capacitor (10 nF) was added to the circuit to perform these measurements. Fig. 3 depicts the typical Lissajous plot obtained during the experiments.

Table 1
Parameters for different reactors at 10 W discharge power. *NC for Not Controlled.

	"Open"		*"Closed"*		*"In tube"*	
	Tap	Oxalic	Tap	Oxalic	Tap	Oxalic
Treated liquid volume, ml	10	10	10	10	1	1
Gas volume, ml	NC	NC	30	30	5	5
Treatment time, min	1–15	1–15	1–15	1–15	0.5–3	0.5–3
Applied voltage, kV	11.0 ± 0.2	10.5 ± 0.2	11.0 ± 0.2	10.5 ± 0.2	12.2 ± 0.2	11.7 ± 0.2
Frequency of the discharge, kHz	30.8 ± 0.3	30.7 ± 0.3	30.8 ± 0.3	30.8 ± 0.3	26.8 ± 0.3	27.6 ± 0.3

In addition, the statistical analysis of the recorded current pulses was also performed. The 10 waveforms with 1 period each for every studied

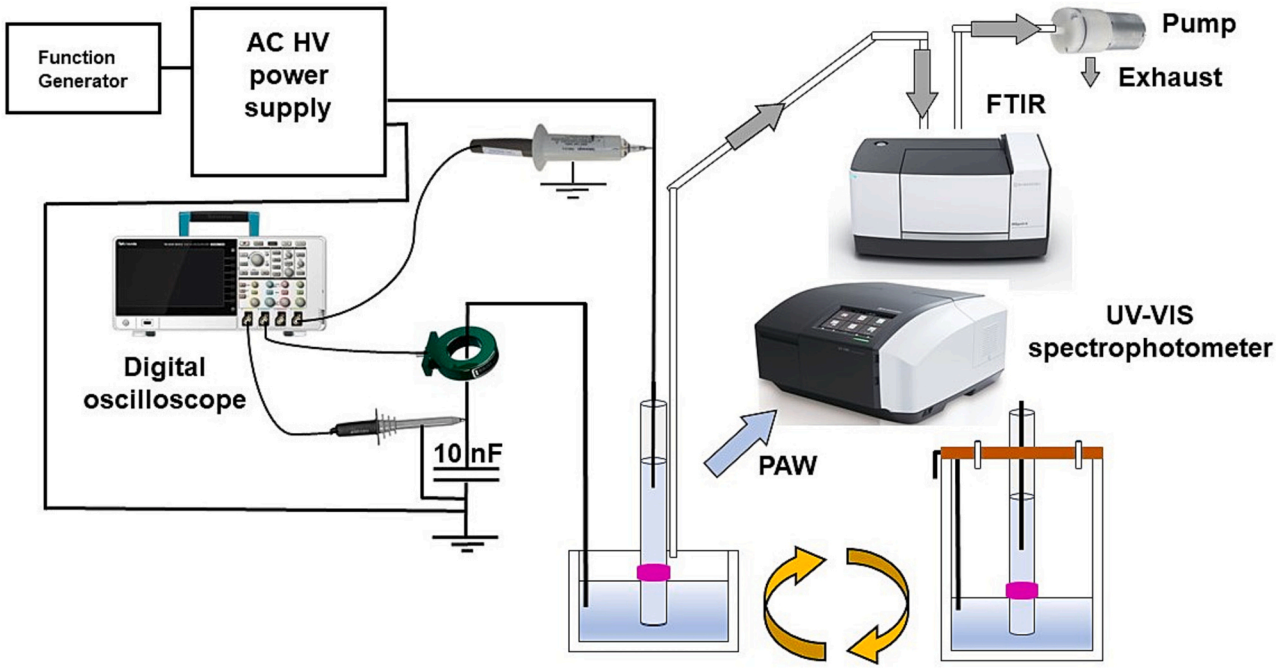

Fig. 2. Schematic of the experimental setup.

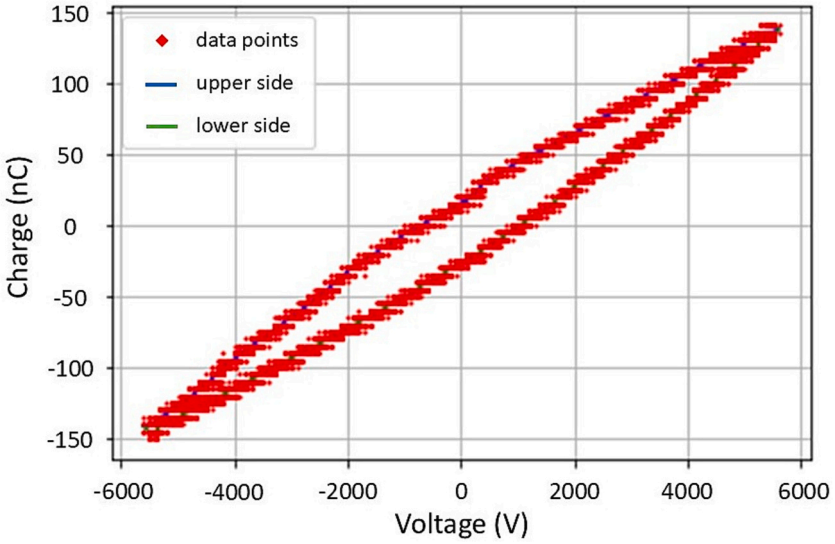

Fig. 3. Example of the Lissajous figure obtained during the plasma treatment of tap water in the *"Open"* reactor.

condition were evaluated. Histograms of current pulses amplitudes were calculated using a self-developed program. The pulse amplitudes were binned at 5 mA intervals to construct the histograms. Pulses above a 10 mA threshold value of either polarity were utilized. This lower limit was implemented to prevent the inclusion of data potentially originating from background electromagnetic interference or minor, random signals induced by the connecting cables' electrical properties. A more detailed explanation of the program algorithm can be found in [26].

2.2. Gas analysis

The gas for the analysis was pumped through a gas tube (PTFE, 6/4 mm) by the air pump with a constant flow rate of 1.3 l min^{-1}. In the *"Open"* and the *"In tube"* reactors, the gas tube was placed ~1 cm above the ground or high-voltage electrode, respectively. In the *"Closed"* reactor, the gas outlet was located on the lid of the reactor chamber (Fig. 1 (c)). In general, the sampling gas flow rate has a substantial influence on the production and accumulation of gaseous species in the plasma reactor. In our work, this gas flow rate was chosen as a compromise between the time needed for filling the FTIR gas cell and the detection limit of the measured species.

The analysis of gaseous species produced by the SDBD was performed by FTIR absorption spectroscopy (*Shimadzu IRSpirit-X*) using a 542 cm long gas cell with ZnSe windows (Fig. 2). The spectra measurement was performed in the middle infrared region of 4000–500 cm^{-1} with a resolution of 0.9 cm^{-1}. The FTIR spectra allowed both qualitative and quantitative identification of various gaseous species generated by SDBD discharge. The concentrations of the gaseous species were evaluated in absolute (ppm) units by modeling the absorption spectra of the species using a set of absorption lines from the HITRAN database (more details can be found in [27]). The following gaseous species were evaluated using the absorption bands as follows: O_3 at 1055 cm^{-1} (LOQ = 7.2 ppm); N_2O at 2235 cm^{-1} (LOQ = 0.6 ppm), N_2O_5 at 742 and 1245 cm^{-1} (LOQ = 0.8 ppm), NO_2 at 1627 and 2916 cm^{-1} (LOQ = 2.1 ppm), and NO at 1900 cm^{-1} (LOQ = 16.4 ppm).

The air relative humidity (RH) was monitored by a capacitive humidity probe (*Arduino*).

2.3. Liquid analysis

The discharge interacting with water solutions facilitates an effective transfer of plasma-generated gaseous reactive species. With the help of UV–Vis absorption spectroscopy (*Shimadzu UV-1800*), the main aqueous species such as hydrogen peroxide H_2O_2, nitrite NO_2^- and nitrate NO_3^- were detected, and their absolute concentrations were evaluated. The presented results are the average of at least five measured samples. The ranges of the calibration curves and the respective R^2 are presented in the supplementary materials. In case the concentrations of the RONS were out of calibration ranges, the samples were diluted to fit the range.

Dissolved ozone ($O_{3(aq)}$) was quantified using the indigo blue assay, a simple and standardized colorimetric method for ozone detection in water and wastewater [28]. Under acidic conditions, $O_{3(aq)}$ rapidly decolorizes the indigo potassium trisulfonate dye, leading to bleaching and formation of the colorless product isatin. The decrease in absorbance at 600 nm ($\varepsilon = 2.38 \times 10^4$ M^{-1} cm^{-1}) correlates linearly with the $O_{3(aq)}$ concentration. As reported previously [29] this method can be susceptible to interference from OH radicals and other reactive oxygen and nitrogen species present in plasma-activated liquids, which may lead to an overestimation of the actual $O_{3(aq)}$ levels.

Hydrogen peroxide (H_2O_2) concentration was determined using the titanium oxysulfate ($TiOSO_4$) assay under acidic conditions [30–32]. In this method, Ti^{4+} ions react with H_2O_2 to form yellow pertitanic acid (H_2TiO_4), exhibiting an absorption maximum at 407 nm, with the color intensity proportional to the H_2O_2 concentration. To prevent H_2O_2 decomposition via reaction with NO_2^- under acidic conditions, PAL samples were immediately stabilized after treatment with 60 mM sodium azide (NaN_3). Sodium azide reduces NO_2^- to molecular nitrogen, thereby preserving H_2O_2 levels [30]. The sample, NaN_3, and $TiOSO_4$ were mixed in a volume ratio of 10:1:5, respectively.

Concentrations of NO_2^- were evaluated by Griess reagents under acidic conditions [33,34] using the chemicals and according to the protocol (Cayman Chemicals Nitrate/ Nitrite Colorimetric Assay Kit # 780001). This method is easy to perform and approved as precise for NO_x^- measurement in the PAL produced by plasma discharge [29]. The reaction of nitrites (NO_2^-) with the Griess reagents leads to the formation of a deep purple azo compound with an absorption maximum of 540 nm.

The total NO_x^- concentration was evaluated by using 10 mM 2,6-xylenol and an acid (H_2SO_4:H_3PO_4 as 1:1) mixture as the reagent. The 10 mM xylenol mixture was prepared by adding 122.16 mg of 2,6-xylenol to 100 ml of 10% glacial acetic acid. The used volume ratio of sample: acid: xylenol was 1:8:1, respectively. The absorption maximum was recorded between 290 nm and 350 nm after subtracting the control in this region. The maximum peak is directly proportional to the concentration of NO_x^-. If the concentration of NO_x^- was too high, we diluted the sample with deionized water to adjust the NO_x^- concentration in the linear absorbance range. Finally, NO_3^- concentration was obtained by

subtracting NO_2^- concentration from NO_x^- concentration [34,35].

3. Results

3.1. General appearance of the discharge and its electrical characteristics

The voltage and current waveforms obtained during electrical measurements of the SDBD in contact with water are presented in Fig. 4. The discharge operated in air contains a large number of small filaments, although almost none of them are visually clearly pronounced, giving the appearance of a diffuse-like discharge. By increasing the power, the discharge becomes more intensive, and the filamentary nature of the discharge becomes more pronounced. As the power increases, so does the discharge current.

The positive polarity half-cycle demonstrates a higher amplitude of current pulses, a phenomenon that has been consistently observed across different types of dielectric barrier discharge systems [36].

Fig. 5 illustrates histograms of positive current pulses for the *"Open"* reactor with tap water and oxalic acid solution as a working liquid. The histograms depict the number of current pulses versus their amplitude for a specified discharge power with vertical logarithmic scales.

The results demonstrate that both the quantity and amplitude of pulses are contingent upon discharge power. Notably, the average number of positive pulses (>10 mA) exhibits a significant increase with rising discharge power. In the oxalic acid solution, the average number surged from approximately 9 ± 2 to 52 ± 8 pulses between 2.5 W and 15 W. Conversely, for tap water, the increase was from 5 ± 1 to 37 ± 2 pulses over the same power range.

When oxalic acid solution is used as an electrode, the discharge current pulses reach higher amplitudes and numbers compared to tap water. When the gas volume near the plasma region is limited, as in the case of a *"Closed"* chamber or especially *"In tube"* reactors, the distribution of amplitudes and number of current pulses changes dramatically.

For comparison, we will further present only the average number of positive pulses and only in an oxalic acid solution. The values obtained after the discharge operation for 9 min in a *"Closed"* reactor were similar to the *"Open"* reactor and were 8 ± 2 and 60 ± 4, for discharge powers 2.5 and 15 W, respectively. However, igniting the discharge within a tube (*"In tube"* reactor) introduced a distinct pattern. While the average number of pulses at lower power (2.5 W) remained comparable to the *"Open"* and *"Closed"* reactors (around 5 ± 2), a significant increase was observed at the highest power (15 W). In this case, the *"In tube"* reactor generated a considerably higher average number of pulses (101 ± 14).

Time-integrated optical emission spectroscopy (OES) measurements were performed; however, quantitative analysis was feasible only for the "Open" reactor configuration. The recorded emission spectra revealed the presence of the second positive system of molecular nitrogen (SPS, N_2 $C^3\Pi_u \rightarrow B^3\Pi_g$), the first negative system of nitrogen ions (FNS, N_2^+ $B^2\Sigma_u^+ \rightarrow X^2\Sigma_g^+$), as well as the vibrational band of OH radicals ($A^2\Sigma^+ \rightarrow X^2\Pi$). Based on the analysis of the N_2 $C^3\Pi_u \rightarrow B^3\Pi_g$ (0–0) band, the rotational temperature at a discharge power of 15 W was estimated to be in the range of 300–350 K. These OES results are presented in the Supplementary Material.

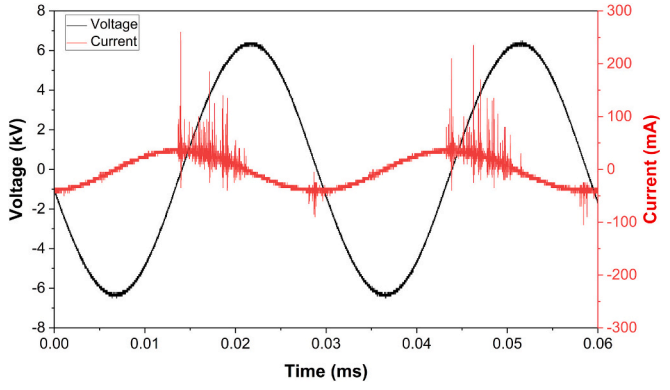

Fig. 4. The typical voltage and current waveforms of the SDBD with liquid electrodes.

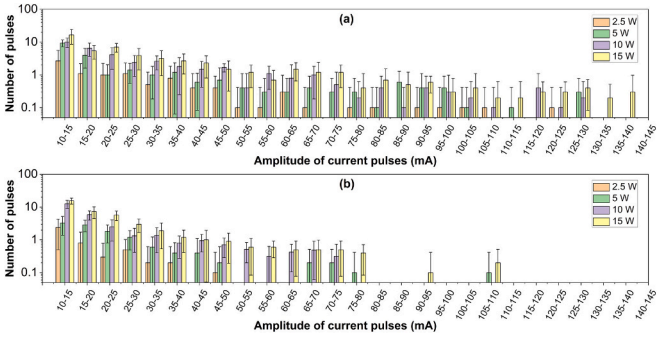

Fig. 5. Amplitude distribution of the positive current pulses of plasma discharge in an *"Open"* reactor while using oxalic acid solution (a) and tap water (b) as a working liquid.

Attempts were also made to acquire OES spectra in the "In-tube" configuration by placing the optical fiber at the top of the test tube, above the active plasma region. Although the detected spectral features were qualitatively similar to those observed in the "Open" reactor, the overall emission intensity was low, which prevented a reliable determination of rotational temperatures. For the "Closed" reactor configuration, OES measurements were not possible due to the presence of a 5 mm thick glass enclosure, which strongly attenuated the emitted radiation and did not allow the acquisition of spectra with a sufficient signal-to-noise ratio.

For a more detailed electrical and optical description of the discharge, please refer to our previous articles, where the optical emission spectroscopy, ICCD imaging, and electrical measurements were performed and discussed in detail [23,24,37].

3.2. Gas phase analysis

3.2.1. Relative humidity

The time evolutions of air relative humidity (RH) for all three reactors with tap water and oxalic acid solution and various discharge powers are presented in Fig. 6. At the lowest discharge power in the *"Open"* reactor, a significantly lower RH increase rate is observed. The results indicate that 2 W is the minimum power required for discharge ignition, with the plasma channels exhibiting the lowest intensity and temperature. In this setting, the RH near the discharge does not exceed 45%.

The most substantial RH increase occurs within 5 min after the discharge ignition. In 15 min, the relative humidity values reached 66 and 69% for tap water and oxalic acid solution, respectively. The results of RH for *"Closed"* and *"In tube"* reactors showed similar trends as the *"Open"* reactor, albeit with variations in the maximal values attained. In the *"Closed"* reactor, the RH eventually reached 100% over time (Fig. 6 (c, d)), while in the *"In tube"* reactor, it was around 80% (Fig. 6 (e, f)).

3.2.2. Ozone production

Ozone concentrations as a function of discharge power for all reactor configurations are shown in Fig. 7. For the *"Open"* reactor, O_3 concentrations with tap water and oxalic acid solution were similar (considering the uncertainties), with maximum concentrations of approx. 128 and 132 ppm, respectively.

In the *"Closed"* reactor, the maximum O_3 concentration was even higher than in the *"Open"* reactor, with a maximum of approx. 143 ppm when using oxalic acid solution. However, with tap water, O_3

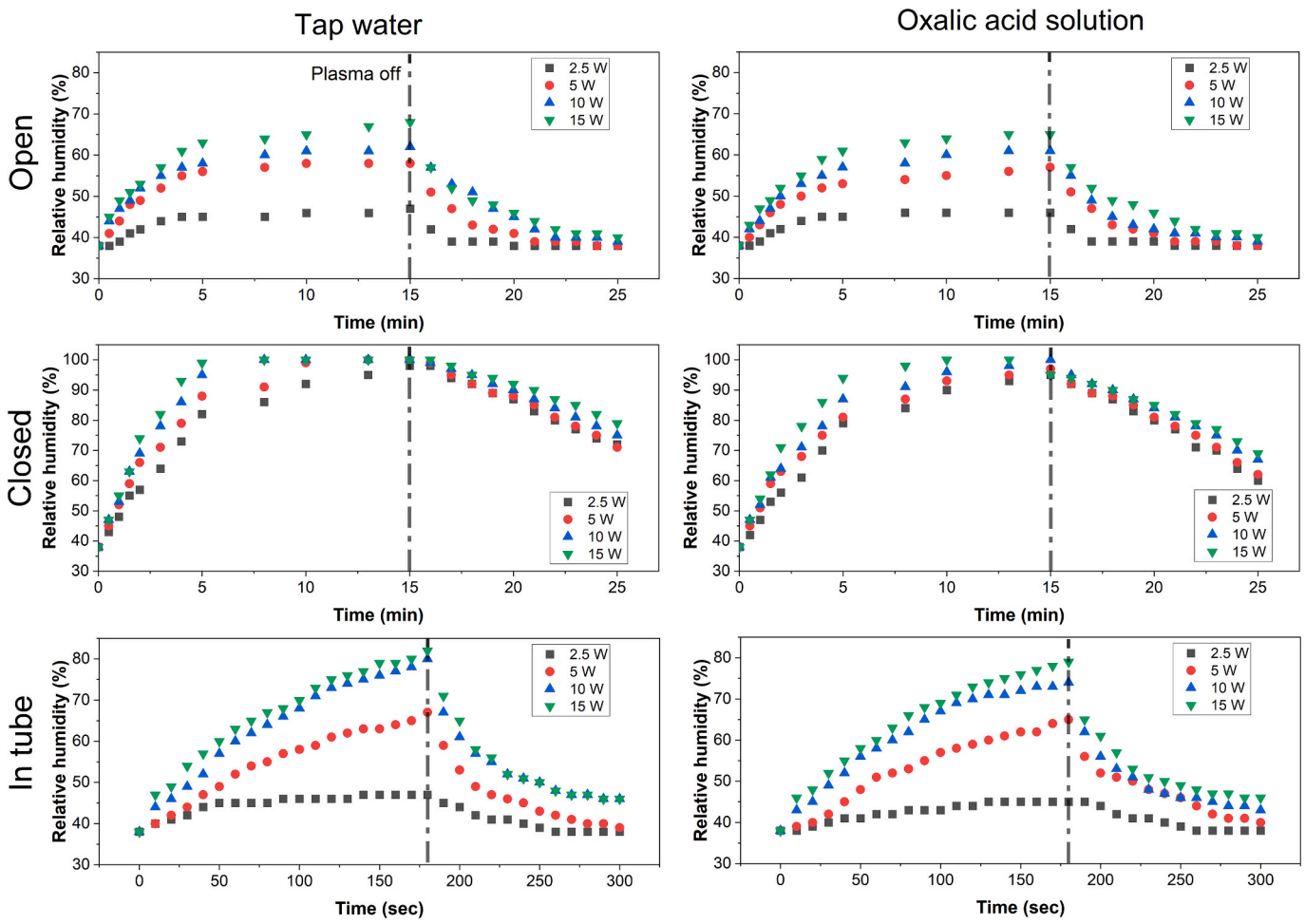

Fig. 6. Time evolutions of air RH for all reactors with tap water and oxalic acid solution and various discharge powers measured. The maximum deviation observed was 2%.

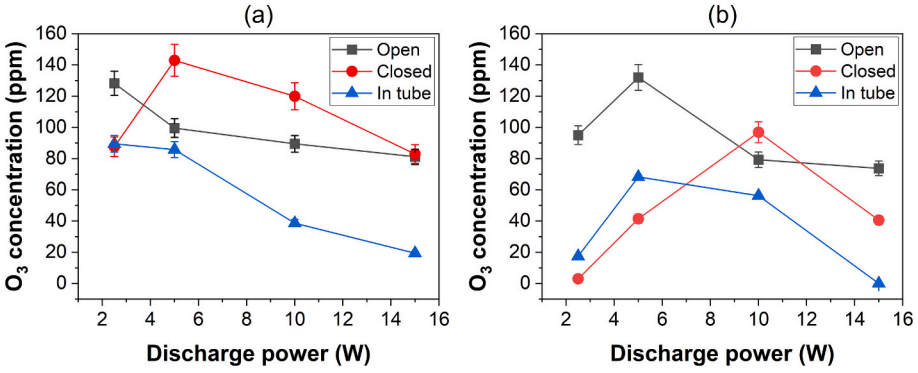

Fig. 7. Ozone concentrations as a function of the discharge power for the *"Open"*, *"Closed"*, and *"In tube"* reactors with an oxalic acid solution (a) and tap water (b) electrodes.

concentrations were mostly lower than those obtained with the *"Open"* reactor.

O_3 production was found to be the lowest in the *"In tube"* reactor. At the highest tested discharge power, the O_3 concentration dropped down eventually to zero (tap water) or close to zero (oxalic acid solution). When oxalic acid solution was used, the maximum O_3 concentration was obtained at lower discharge powers in contrast to tap water in all reactors.

3.2.3. Nitrous oxide production

Fig. 8 summarizes the measured N_2O concentrations for all reactors. In the case of the *"Open"* reactor, N_2O concentration was low (approx. 2 ppm) and stable in the whole range of tested discharge power for both working liquids.

In the *"Closed"* and the *"In tube"* reactors, the N_2O concentrations were higher, probably as a result of more efficient gas sampling. The concentrations increased monotonously and almost linearly with increasing discharge power. The use of oxalic acid solution resulted in higher N_2O concentrations across the whole range of discharge power.

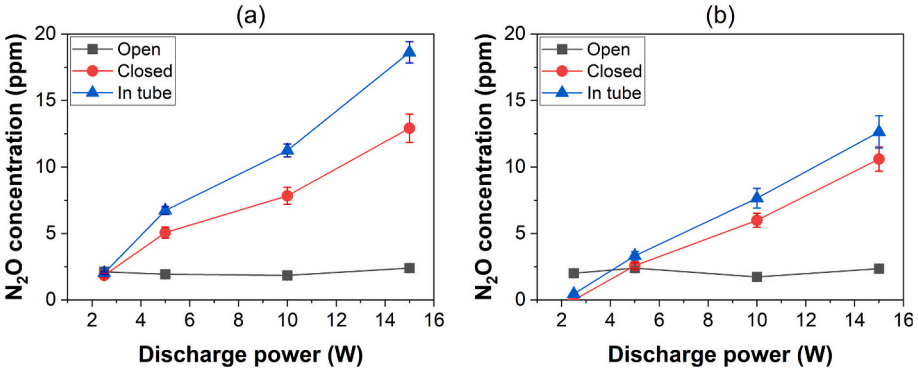

Fig. 8. Nitrous oxide N_2O concentration as a function of the discharge power for *"Open"*, *"Closed"*, and *"In tube"* reactors with an oxalic acid solution (a) and tap water (b) electrodes.

The highest N_2O concentrations were obtained in the *"In tube"* reactor for the highest discharge power of 15 W (approx. 19 and 13 ppm with oxalic acid solution and tap water, respectively).

3.2.4. Dinitrogen pentoxide and nitrogen dioxide production

NO was not detected at all under the tested experimental conditions in our work, whereas NO_2 was only observed in the *"In tube"* reactor at maximum discharge power. On the other hand, N_2O_5 was always detected as a result of further oxidation of NO_2.

Fig. 9 shows N_2O_5 concentration as a function of discharge power for all reactors, with a pattern almost identical to N_2O. For the *"Open"* reactor, the concentrations were low (from approx. 0.5 to 1.3 ppm) and quite stable in the whole range of discharge power for both working liquids. In both *"Closed"* and *"In tube"* reactors, the N_2O_5 concentrations increased with increasing discharge power, with higher values obtained with oxalic acid solution. The maximum N_2O_5 concentrations of approx. 5.3 and 2.4 ppm were found in the *"In tube"* reactor with oxalic acid solution and tap water, respectively.

Neither HNO_2 nor HNO_3 was detected in the gas phase under all tested conditions.

3.3. Liquid phase analysis

For the measurements of RONS concentrations in liquids treated by the SDBD in the three reactors, the treatment time and input power were used as changing parameters to investigate the time evolution of RONS production rates.

The findings indicate that the production of RONS in liquids within the *"Open"* reactor does not exhibit a discernible dependence on the treatment time or the input power. Instead, it is concluded that the deposited energy per liquid volume (power x treatment time, divided by the liquid volume) plays a pivotal role in RONS generation. For the unification of data measured for all the variable parameters, we will present the dependence of RONS concentrations as a function of energy deposited in a ml of liquid (J/ml), while the highest discharge power (15 W) was used.

In the "*Closed*" and "*In-tube*" reactor configurations, the evolution of some liquid-phase species with deposited energy density (J/ml) can be approximated by a simple empirical kinetic model. For example, H_2O_2 concentration followed an approximately first-order trend with respect to deposited energy, showing no statistically relevant difference between conditions employing lower power over longer durations and higher power over shorter durations when the total energy input was equivalent. This suggests that, for this species, the cumulative energy delivered to the system is the dominant controlling factor.

By contrast, in the tap water, dissolved ozone ($O_{3(aq)}$) and, to a lesser extent, NO_2^- exhibited a modest sensitivity to the specific power–time combination. In general, lower discharge power applied over longer treatment times resulted in slightly higher concentrations compared to higher power applied over shorter times, even at identical energy densities. This behavior is consistent with enhanced gas–liquid mass transfer over extended interaction times, combined with progressive humidity build-up and increased gas residence time in the confined reactor volumes. Considering also the buffering capacity and chemical composition of the tap water used in this study, the resulting higher concentrations of $O_{3(aq)}$ and NO_2^- under these conditions are physically reasonable.

Although these trends were reproducible, the magnitude of the

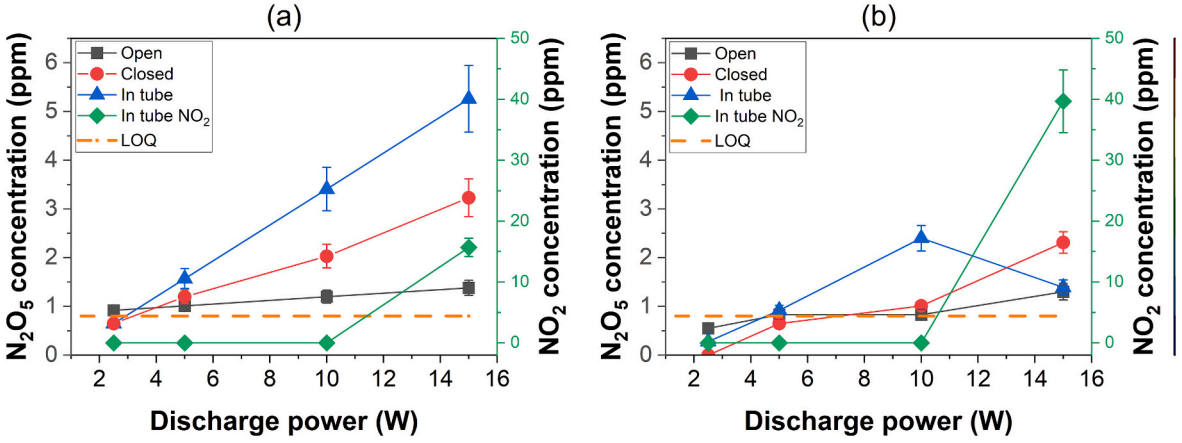

Fig. 9. Dinitrogen pentoxide N_2O_5 and nitrogen dioxide NO_2 concentrations as a function of the discharge power for *"Open"*, *"Closed"*, and *"In tube"* reactors with an oxalic acid solution (a) and tap water (b) electrodes.

observed differences in $O_{3(aq)}$ and NO_2^- concentrations was relatively small."

3.3.1. Temperature

To optimize the treatment parameters and tailor them to specific material properties or desired process outcomes, it is required to understand how reactor design and treatment duration influence the thermal response of the liquid and polymer during the plasma treatment. The temperature evolution depends on the applied voltage, the liquids used, the dielectric thickness, as well as the treatment speed. In this study, we present a simplified version of this process, where the dielectric remains stationary. The evolution of liquid temperatures in the studied reactors under these conditions was recorded. In the *"Open"* and *"Closed"* reactors, the experiments lasted for 15 min, while in the *"In tube"*, the maximum duration was 3 min due to the substantially lower volume of the treated liquid.

The temperature of the oxalic acid solution reached 30 °C, 37 °C, and 30 °C for *"Open"*, *"Closed"*, and *"In tube"* reactors, respectively. The temperature of tap water under the same conditions reached 36 °C, 39 °C, and 30 °C, respectively.

The observed differences persist consistently over time and across various applied powers. While the difference between the two liquids is relatively low, it remains constant throughout the experiments. This suggests that the choice of liquid influences the heating dynamics and plasma characteristics in the system.

3.3.2. pH changes

The liquids used as electrodes significantly differ in pH. Tap water, prior to discharge ignition, maintains a pH of 7.8, while the oxalic acid solution exhibits a significantly lower pH of 1.5 (Fig. 10). These pH values stay constant over the treatment duration in an *"Open"* reactor. A different trend is observed in the *"Closed"* reactor, where a progressive decrease in pH occurs during the plasma treatment, with liquid condensation occurring on reactor walls after 10–15 min of operation. Further intensification of pH reduction is observed in the *"In tube"* reactor, where a significant pH drop is detectable within the first 10 s of plasma exposure. Oxalic acid solution retains its constant pH = 1.5 in all three reactors.

3.3.3. Ozone in liquid phase

The *"Open"* reactor demonstrates a continuous and nearly linear increase in $O_{3(aq)}$ concentration with increasing energy input (Fig. 11).

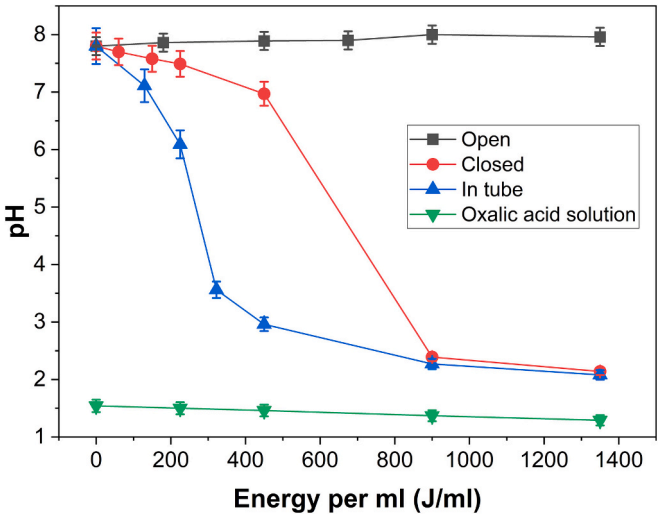

Fig. 10. pH as a function of the energy density for *"Open"*, *"Closed"*, and *"In tube"* reactors with tap water electrodes, compared with pH in oxalic acid solution (all reactors).

At the maximum applied energy density (~1400 J/ml), the $O_{3(aq)}$ concentration reached 300 μM. The *"Closed"* reactor shows a small initial $O_{3(aq)}$ increase up to ~400 J/ml in oxalic acid solution, but then it declines. The $O_{3(aq)}$ concentration in tap water is nearly undetectable. Similarly, the *"In tube"* reactor maintains a relatively stable $O_{3(aq)}$ concentration (~50 μM) in oxalic acid solution, whereas in tap water it does not exceed 25 μM.

3.3.4. Hydrogen peroxide in liquid phase

Fig. 12 depicts the dependence of H_2O_2 concentration on the input energy delivered into the liquid during the plasma treatment with all three tested reactors. With increasing energy input, there is a linear increase in the concentration of H_2O_2. The highest concentration of H_2O_2 is more than 3200 μM at the maximum energy used while using the oxalic acid solution as the liquid electrode.

In contrast to oxalic acid, Fig. 12 (b) shows much lower H_2O_2 concentrations in tap water, but again, there is a gradual increase with the energy input. Unlike with oxalic acid, it is the *"Open"* reactor that produces the highest peroxide concentrations, followed by the *"In tube"* and *"Closed"* ones.

3.3.5. Nitrites in liquid phase

In oxalic acid solution, NO_2^- concentration increases with the rising energy input for the *"Open"* and *"In tube"* reactors (Fig. 13). The *"Open"* reactor exhibits the most significant rise in NO_2^- concentration, reaching approximately 250 μM at 1400 J/ml. The *"In tube"* reactor follows a similar trend but with slightly lower values. In contrast, the *"Closed"* reactor shows almost zero accumulation of NO_2^- at every energy input level.

For tap water, the trends are distinctly different from those of oxalic acid solution. The *"Open"* reactor leads to the highest NO_2^- concentrations, reaching around 700 μM at 1400 J/ml. The *"In tube"* reactor also demonstrates the same increase up to ~800 J/ml, and after that, the NO_2^- concentration becomes constant and then declines slightly. For the *"Closed"* reactor, NO_2^- concentrations remain significantly lower, peaking around 400 J/ml before declining.

3.3.6. Nitrate in liquid phase

Fig. 14 indicates the relationship between nitrate ion (NO_3^-) concentration and energy input per milliliter in the two studied liquids. In Fig. 14 (a), in oxalic acid solution, the concentration of NO_3^- exhibits a clear increasing dependence on the energy input. The *"Closed"* reactor demonstrates a significant increase in NO_3^- concentration, reaching approximately 8 mM at the highest energy input of 1400 J/ml. Compared to this, the *"Open"* and *"In tube"* reactors record a significantly lower increase, with *"In tube"* slightly higher than *"Open"*. The observed differences suggest that the *"Closed"* reactor enhances the retention of nitrogen-based reactive species, leading to a higher conversion to NO_3^-.

For tap water, the same trend is observed, with the *"Closed"* reactor recording the highest NO_3^- concentration of approximately 7 mM for the maximum energy input. The overall NO_3^- concentrations in tap water are lower than those in oxalic acid solution, particularly for the *"Open"* and *"In tube"* reactors.

4. Discussion

4.1. Electrical characteristics and discharge behavior

The electrical characteristics of the SDBD system reveal several important phenomena that directly influence the plasma-liquid interactions and subsequent chemical processes both in the gas and the liquid. The positive polarity half-cycle demonstrates a higher amplitude of current pulses, a phenomenon aligning with the established electrical characteristics of discharges seen in SDBD actuators [38]. This observation is supported by similar findings in related studies, indicating a

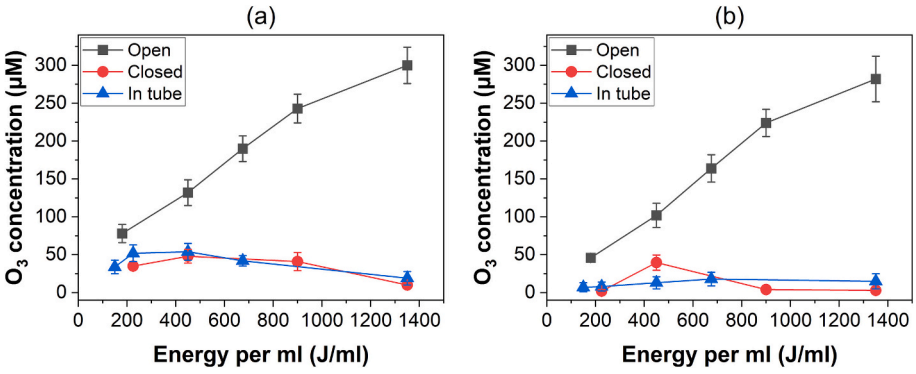

Fig. 11. Ozone concentration in liquid as a function of the energy density for *"Open"*, *"Closed"*, and *"In tube"* reactors with an oxalic acid solution (a) and tap water (b) electrodes.

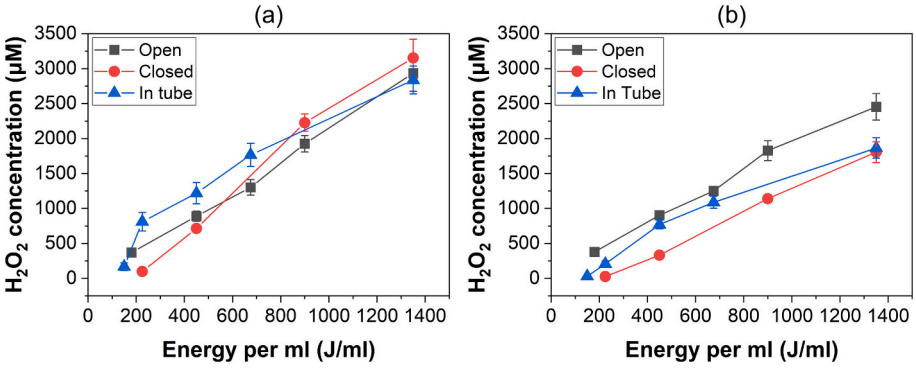

Fig. 12. Hydrogen peroxide concentration in liquid as a function of the energy density for *"Open"*, *"Closed"*, and *"In tube"* reactors with an oxalic acid solution (a) and tap water (b) electrodes.

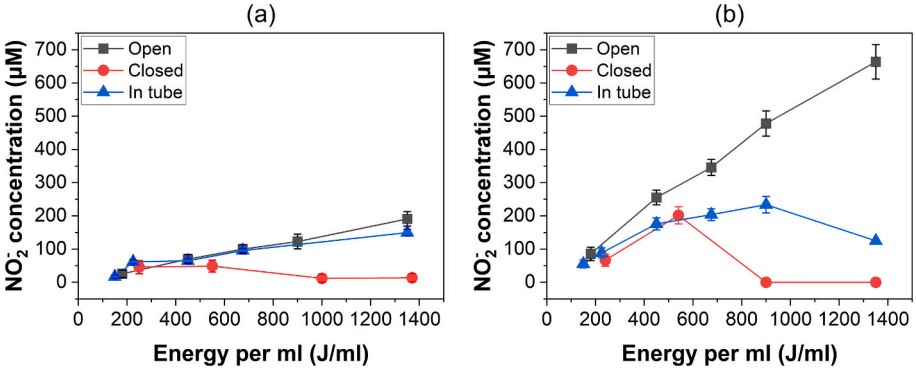

Fig. 13. Nitrite concentrations in liquid as a function of the energy density for *"Open"*, *"Closed"*, and *"In tube"* reactors with an oxalic acid solution (a) and tap water (b) electrodes.

consistent pattern across different types of dielectric barrier discharge systems [36].

The enhanced discharge performance when using oxalic acid solution compared to the tap water as a liquid electrode can be explained by the fact that the oxalic acid solution is more conductive, resulting in higher charge transfer through the plasma channels. This increased conductivity leads to more intense discharge conditions, which subsequently affect both gas-phase and liquid-phase chemistry.

The dramatic changes observed in current pulse distribution when gas volume is limited (in *"Closed"* or *"In tube"* configurations), can be mainly explained by changes in gas humidity. Right after the discharge ignition in both *"Closed"* and *"In tube"* reactors, the current pulse distribution is the same as in the case of the *"Open"* reactor. As humidity progressively increases, the amplitude of current pulses decreases.

A similar effect was also observed by other researchers. For example, in [39], the authors reported that in surface dielectric barrier discharge plasma operated in small chambers for water treatment, the evaporation of liquid water enhances and, thus, increases the air humidity, which in turn significantly affects the electrical characteristics of the discharge and the plasma generation rates of primary reactive species.

The air humidity affects multiple aspects of the discharge: it decreases the peak current of the discharge and the number of microdischarges, thus reducing the plasma volume within the reactor [40]. Additionally, it affects the distribution of the electric field [41], microdischarge intensity, the mobility of charge carriers [42], and power loss in the dielectric material [43]. It further reduces the surface resistance of

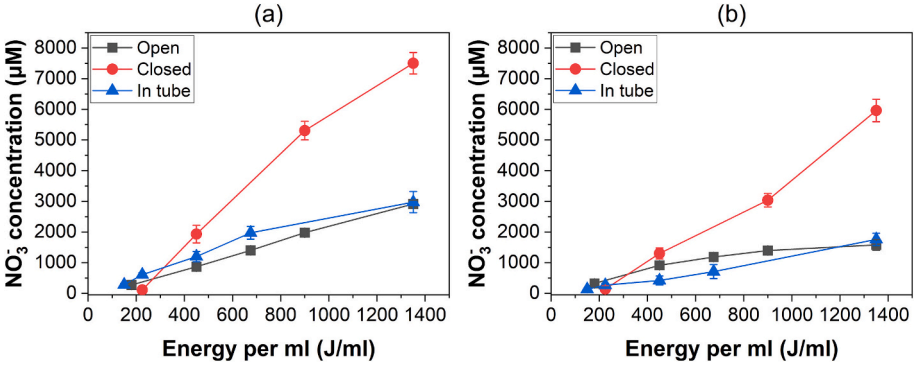

Fig. 14. Nitrate concentrations in liquid as a function of the energy density for *"Open"*, *"Closed"*, and *"In tube"* reactors with oxalic acid solution (a) and tap water (b) electrodes.

the dielectric due to water adsorption [40] and the total charge transfer per half-period of the applied voltage [40,43].

4.2. Gas phase chemistry and humidity effects

Generating the non-thermal plasma discharge in ambient air is advantageous for most of applications as it provides a low-cost, yet highly effective source of oxygen O_2 and nitrogen N_2. During the discharge generation in air, many gaseous species are produced. The primary species are produced by electron impact on double-bonded O_2 and triple-bonded N_2 molecules and, in particular, include atomic oxygen (·O) and nitrogen (·N), as well as excited nitrogen molecules (N_2*). Excited N_2* can be dissociatively quenched by molecular O_2, leading to the additional production of atomic oxygen ·O with high probability. Additionally, high-energy electrons can ionize N_2 and O_2 molecules, generating O_2^+ and N_2^+ ions. These ions may further react through dissociative electron–ion recombination reactions, also contributing to the production of atomic ·O and ·N species [44].

The primary species in the gas phase may be subject to interactions with each other, resulting in the production of several gaseous secondary species, including ozone O_3, nitric oxide NO, nitrogen dioxide NO_2, nitrous oxide N_2O, nitrous acid HNO_2, nitric acid HNO_3, etc. [11]. If the discharge is in contact with a liquid (e.g., water or water solution), the gaseous secondary species can dissolve in it, inducing further chemical reactions. As a result, many aqueous RONS (·OH, H_2O_2, NO_2^-, NO_3^- or ONOOH) are formed in PAL [1]. Moreover, the presence of a liquid in a plasma reactor influences the air humidity, which further substantially modifies the gas-phase plasma chemistry.

The application of higher discharge power leads to an increased temperature, thus higher evaporation and an increase in RH, eventually leading to RH saturation. This outcome aligns with our expectations regarding the relationship between the power input and the humidity dynamics.

It is important to note that, unlike *"Open"* and *"Closed"* reactors, direct measurement of RH near the plasma region was not feasible in the *"In tube"* reactor. Instead, RH was measured at the reactor outlet during FTIR measurements, leveraging the presence of applied gas flow. The introduction of the sampling gas flow significantly altered the measured RH value parameters in the *"In tube"* reactor. This gas flow was necessary for the remote FTIR measurements, and its rate was carefully controlled to maintain a reasonably low value. However, the limited gas volume inside the test tube resulted in nearly constant gas exchange near the plasma region. For this reason, we did not achieve the humidity saturation in the *"In tube"* reactor within the duration of the experiment. However, it is evident that the behavior at the lowest discharge power mirrors that observed in the *"Open"* reactor. The values of RH obtained surpass those of the *"Open"* reactor, as anticipated due to the restricted gas volume within the test tube, and closely align with the values of the *"Closed"* reactor during identical treatment times (except for the lowest discharge power of 2.5 W). Finally, the results proved a substantial increase of air RH during the discharge operation that consequently strongly influences the formation of gaseous species. The same effect was also experimentally observed by other authors using the SDBD generated over the water surface [39], as well as by numerical simulations [45].

Measurements of RONS in the liquid, on the other hand, were conducted without the sampling air flow in the *"In tube"* reactor to better approximate the real scenario of the plasma-liquid interaction.

4.2.1. Ozone formation and decomposition mechanisms

The production of O_3 is a typical phenomenon occurring in DBD air discharges [11]. The atomic oxygen ·O is first produced by electron-impact and further O_3 formation takes place via a three-body reaction. The presence of water vapors in the air substantially decreases the O_3 concentration through direct reactions of O_3 with water-derived H, OH, and HO_2 radicals [46]. Another explanation for decreasing O_3 concentration in humid air includes the consumption of atomic oxygen ·O that is essential for O_3 production in reactions with OH and HO_2 radicals [47]. In the presence of a discharge, the O_3 molecules are formed and at the same time dissociated mostly by thermal decomposition, electron impact reaction, UV absorption, and reactions with atomic or molecular oxygen or nitrogen oxides (NO, NO_2) [48,49].

Therefore, the air humidity, along with other effects described above (O_3 thermal decomposition, electron impact reaction, and consumption of atomic oxygen O), may be expected to have a significant influence on the O_3 production. This applies in particular to plasma reactors employing liquid water or water solutions, which may exhibit significant evaporation during the discharge operation. Moreover, all these effects become more dominant as the discharge power increases, leading to a gradual O_3 decomposition and a decrease in its concentration that was observed for all tested reactors.

The higher O_3 production observed in the *"Closed"* reactor with oxalic acid solution, despite the highest air RH, suggests that the more intense discharge, accompanied by a higher number and higher amplitude of current pulses (see Section 3.1) dominated over the adverse effect of higher humidity. However, the negative effect of high RH was found dominant with tap water (Fig. 7 (b)), as O_3 concentrations were mostly lower than those obtained with the *"Open"* reactor.

The lowest O_3 production in the *"In tube"* reactor (Fig. 7) is a consequence of the intense gas exchange in the test tube due to a large gas flow for such a small gas volume inside the tube. The transition of the discharge from "ozone O_3 mode" to "nitrogen oxides NO_x mode" at the highest discharge power, accompanied by a complete depletion of O_3 and the increase of NO and NO_2 [50], occurs when the NO_x concentration reaches the level at which atomic oxygen ·O reacts faster with NO and NO_2 than with O_2 to form O_3 [51]. Park et al. [52] observed a direct relation between the gas temperature and the discharge mode transition. Therefore, we suppose the transition is a result of high gas temperatures

near the plasma channels in a confined gas volume inside the test tube that modified the prevailing reactions and transitioned the discharge into the "NO_x mode".

Other experimental studies demonstrate that a higher gas temperature, together with a higher air RH, may be jointly responsible for the observed decrease in O_3 production with increasing discharge power. In our experiment, when oxalic acid solution was used, the maximum O_3 concentration was obtained at lower discharge powers in contrast to the tap water in all reactors (Fig. 7). This effect may also be related to a more intense discharge when using oxalic acid solution as a working liquid.

4.2.2. Nitrogen species formation

Other typically expected gaseous products of atmospheric-pressure air DBDs are nitrogen oxides, especially N_2O at lower power densities, and NO and NO_2 [49]. The formation of nitrogen oxides follows complex pathways that are significantly influenced by temperature and humidity conditions. N_2O is formed by the reaction of N_2 with atomic O and typically accompanies O_3 formation under the same conditions. The primary formation of NO is given by the Zeldovich mechanism [53] that requires higher gas temperatures, which is followed by subsequent NO oxidation to NO_2 [54].

However, NO was not detected at all under the tested experimental conditions in our work, whereas NO_2 was only observed in the *"In tube"* reactor at maximum discharge power. Instead, N_2O_5 was always detected as a result of further oxidation of NO_2 by O_3 [55]. Even if some NO and NO_2 were present in the gas without being oxidized to N_2O_5, their concentrations were below the detection limit of the setup (approx. 4.9 ppm for NO and 0.6 ppm for NO_2).

Abdelaziz et al. [56] found that the surrounding gas temperature significantly influences the selectivity of nitrogen-containing products. They further noted that higher oxidation states of nitrogen are more readily produced at lower temperatures, whereas operating SDBD at elevated temperatures enhances selectivity for NO. Therefore, the absence of NO and NO_2 in the FTIR spectra (except for the *"In tube"* reactor) may indicate the relatively low gas temperature in the reactors during the discharge operation, which favors the oxidation of low concentration NO and NO_2 to N_2O_5 via reactions with much more abundant O_3. The same effect was also observed by Kogelschatz and Baessler [55].

Additionally, as previously mentioned, the transition from "O_3 mode" to "NO_x mode" in the *"In tube"* reactor occurred at the highest discharge power of 15 W. Here, depletion of O_3 resulted in the lower formation of N_2O_5 and the associated increase of NO_2 concentration. Since a full O_3 consumption was observed only over tap water (Fig. 7 (b)), a more significant decrease of N_2O_5 and higher NO_2 concentration with a maximum of approx. 40 ppm were observed with tap water electrode (Fig. 9 (b)). With the oxalic acid solution, there was still some remaining O_3 in the reactor (approx. 19 ppm), so N_2O_5 was not strongly affected and, thus, NO_2 concentration was lower (approx. 16 ppm).

Under humid air conditions, further oxidation of NO_x, promoted by water-derived OH and HO_2 radicals, can lead to the formation of HNO_2 and HNO_3 [27,57]. Nevertheless, neither HNO_2 nor HNO_3 was directly detected in the gas phase under all tested conditions. The reason for that could be their rapid dissolution in the present liquid and formation of NO_2^- and NO_3^- ions due to their very high Henry's law solubility coefficients, with low remaining concentrations in the gas phase [58], under the detection limit. The production rate of NO_2^- and NO_3^- in the liquid that is directly formed upon entering HNO_2 and HNO_3 into water was found to be 30 μM and 140 μM per minute. Considering their high Henry's law coefficients, their remaining gas concentrations should be below 1 ppm, which is below the detection limit of the experimental setup.

4.3. Liquid phase chemistry and RONS formation

4.3.1. Temperature and pH effects on liquid chemistry

The temperature differences observed between different liquids and reactor configurations have significant implications for chemical processes. The choice of liquid significantly influences the heating dynamics and plasma characteristics in the system. The relatively modest temperature increase (maximum 39 °C) ensures that thermal decomposition effects remain limited, allowing chemical processes to be dominated by plasma-induced reactions rather than thermal effects.

The pH behavior reveals important insights into the chemical processes occurring in different reactor configurations. Contrary to the anticipated decrease in pH observed in most of the plasma-treated deionized or distilled water, where strong acidification occurs [30], the pH of the treated tap water in the *"Open"* reactor was not changed and remained constant (within the error range) during our experiments. This can be explained by a relatively strong natural bicarbonate/carbonate buffer system in the used tap water. This is due to the fact that the bicarbonates (HCO_3^-) and carbonates (CO_3^{2-}) react with the hydrogen ions (H^+) contributed by the acid, preventing them from dropping the pH [59], as typically occurs in plasma-activated deionized water. However, slight pH changes using tap water were also reported [60] typically after longer treatment times [61].

To verify the assumed buffering capacity of the tap water, an additional titration test with HNO_3 was performed, yielding an alkalinity of around 208 mg/l (4.16 mM). The dependence of pH on the added volume of 15 mM HNO3 solution showed a gentle slope in the region between 0 and 15 ml in the region 18–20 ml curve starts to bend more steeply, and at 20–30 ml, the pH drops very fast. The corresponding titration curve (pH vs. added HNO_3) is provided in the Supplementary Material. This evaluation supports the observed stability of pH in the "*Open*" configuration.The progressive pH decrease in the *"Closed"* reactor results from altered humidity and temperature dynamics in the plasma region, leading to liquid condensation on reactor walls and elevated concentrations of reactive nitrogen species. Further intensification of pH reduction is observed in the *"In tube"* reactor (Fig. 10), where a significant pH drop is detectable within the first 10 s of plasma exposure. Unlike the *"Open"* reactor, where the buffer effect stabilizes pH, the confined gas and low liquid volume in the *"In tube"* reactor facilitate rapid acidification, which is related to significantly higher NOx production and accumulation.

Oxalic acid solution retains its constant, already low pH = 1.5 in all three reactors.

4.3.2. Oxygen species chemistry in the liquid phase

The formation of different RONS species follows distinct pathways that are influenced by reactor configuration, liquid properties, and operating conditions. Ozone in liquid originates primarily from gas-phase O_3 dissolution, as $O_{3(aq)}$ is not directly produced in water [62]. Although $O_{3(aq)}$ has a small Henry's law constant, $H^{cp} = 1.0 \times 10^{-4}$ mol/(m^{3}Pa) (much smaller than that of OH 3.8×10^{-1} mol/(m^{3}Pa) and H_2O_2 8.3×10^2 mol/(m^{3}Pa)) [63], its presence in the gas phase can still result in a measurable concentration of $O_{3(aq)}$.

The variation in $O_{3(aq)}$ concentration between different liquids can be attributed to the interplay of temperature and pH, impacting the solubility and reactivity of O_3 within the treated liquid. Previous research by Sotelo [64] established a clear link between temperature, pH, and the solvation of $O_{3(aq)}$. Their findings demonstrated that increasing the liquid temperature leads to a decrease in $O_{3(aq)}$ solvation. However, the impact of pH was found to be even stronger, with a significant rise in $O_{3(aq)}$ solvation observed at lower pH values. For example, the approximate solvation values of 3.2×10^4 mol/l and 2.5×10^4 mol/l at pH 7 and 8, respectively, were reported [64]. Notably, a substantial increase to 5.7×10^4 mol/l was observed when the pH was lowered to 2.5.

The authors assume that the main reason for the $O_{3(aq)}$ decrease is the increased humidity in the chamber and the liquid temperature. As it is seen from the gas phase analyses, the recorded O_3 concentrations decreased with the increased applied power (Fig. 7). Higher concentrations of NO_x species in the liquid that react with $O_{3(aq)}$ could also be a reason for the decrease in $O_{3(aq)}$ concentration.

Hydrogen peroxide H_2O_2, is produced mostly in the gas phase by 3-body recombination of ·OH radicals and subsequently dissolves into the water very quickly due to its extremely high Henry's law solubility. O'Sullivan et al. [65] investigated the behavior of several Henry's law constants and showed that H^{cp} of H_2O_2 decreased with increasing temperature, however, remained unaffected by the changes in pH.

The linear increase in H_2O_2 concentration with energy input in all reactor configurations confirms that H_2O_2 production is primarily limited by the availability of ·OH radicals rather than dissolution kinetics. The difference in H_2O_2 concentrations between oxalic acid and tap water can be attributed to peroxynitrite formation,

$$H_2O_2 + NO_2^- + H^+ \rightarrow ONOOH + H_2O \quad (1)$$

which consumes H_2O_2 and leads to reduced steady-state concentration in acidic environments. This explains why in the very acidic environment of oxalic acid solution, all three reactors perform similarly, whereas in tap water, lower H_2O_2 is observed in the *"Closed"* and *"In-tube"* reactors.

4.3.3. Nitrogen species chemistry in the liquid phase

The formation of nitrite and nitrate ions in the liquid phase involves complex chemistry that is strongly dependent on pH conditions. The stable pH = 7.8 of tap water in the *"Open"* reactor suggests a dominant peroxone process,

$$H_2O_2 + 2O_3 \rightarrow 2\cdot OH + 3O_2 \quad (2)$$

where hydrogen peroxide reacts with ozone to form hydroxyl radicals, influencing the NO_2^- dynamics so that NO_2^- cannot so readily react with H_2O_2.

In the oxalic acid solution with pH = 1.5, primary reactions involve acidic disproportionation of $NO_{2(aq)}^-$ to $NO_{3(aq)}^-$

$$3NO_2^- + 2H^+ \rightarrow 2NO + NO_3^- + H_2O \quad (3)$$

and peroxynitrite formation (1) and its subsequent decay pathways:

$$ONOOH \rightarrow NO_3^- + H^+ \quad (4)$$

$$ONOOH \rightarrow \cdot OH + \cdot NO_2 \quad (5)$$

Under acidic conditions, nitrite ions react at much higher rates compared to basic or neutral conditions. This observation is further supported by data presented in Fig. 14 (b), showing significantly higher nitrate ion levels in the *"Closed"* reactor compared to the *"Open"* reactor. The significant increase in NO_3^- concentrations in the *"Closed"* reactor could also be partly attributed to higher efficiency in nitrogen species retention, by limiting exposure to ambient air.

4.4. Comparison with previously reported similar studies

To contextualize our findings, a comparative analysis with existing literature was carried out, focusing on the efficiency of RONS production. The comparison with existing literature reveals significant variations in RONS concentrations under different plasma reactors and treatment conditions. These variations highlight the importance of considering the unique role of individual plasma arrangements in affecting the water treatment outcomes.

The referenced studies were carefully selected based on their use of similar plasma types and reactor configurations, allowing for a more meaningful evaluation of the performance and effectiveness of our system.

We first discuss studies employing surface dielectric barrier discharges. It should be noted, however, that with the exception of the present work, most SDBD configurations do not involve direct contact with the liquid. We then turn our attention to dielectric barrier discharges in direct contact with the liquid, as our discharge is also filamentary in nature and operates in a liquid-contact configuration.Xu et al. [66] showed that the change in the plasma-chemistry mode (O_3-dominant to NO_x-dominant) was more sensitive to the metal ground-electrode temperature above the treated liquid than to the power density and the gas temperature. O_3 in the gas and liquid phases could not be detected at electrode temperatures above 90 °C. We can suggest that a similar effect also takes place in our *"Closed"* reactor. As the plasma is ignited in the same region of the glass tube for 15 min (in contrast to the projected application of catheters/tubes disinfection, where the dielectric tube will be moving), the tube gets heated up to 80–90 °C for the higher input powers used in this study. Notably, tap water undergoes a faster total degradation of the dissolved ozone compared to the oxalic acid solution. Xu et al. [66], used a plasma reactor with 6 W power SDBD and chamber dimensions similar to the one used in our study. Surprisingly, their measured RONS concentrations were much lower compared to our reactors, even though the setups were alike. The position of the plasma reactor, 5 mm above the liquid surface in their setup, could be one reason for this difference. This difference in setup might affect how the plasma interacts with the liquid and, in turn, influence RONS production.

The SDBD setup reported by R. Agus [67] applied above the water surface can be considered analogous to our "Closed" reactor configuration. Agus et al. treated 150 ml of liquid for up to 30 min, with an 8 mm gap between the plasma and the liquid and a power input of 39 W. The closest comparable condition to our setup is the static treatment for 30 min, under which they reported concentrations of H_2O_2, NO_2^-, and NO_3^- of 7 μM, 670 μM, and 940 μM, respectively.

In comparison, our results show a considerably higher H_2O_2 concentration (330 μM), higher NO_3^- (1400 μM), and a much lower NO_2^- concentration (200 μM) (see Fig. 15). These differences can likely be attributed to peroxynitrite formation. In the system described by Agus et al., the very low H_2O_2 concentration would have limited this reaction pathway, preventing significant consumption of NO_2^-. In our case, the higher availability of H_2O_2 likely promoted peroxynitrite formation, thereby reducing the NO_2^- concentration and shifting the balance of reactive nitrogen species toward NO_3^-.

A similar configuration was also reported in another study [68], where airflow was introduced and shorter exposure times (10 s to 5 min) were applied at a plasma power of 7.75 W, with a reduced gap of 3 mm between the electrode and the liquid surface. Compared with this work, our setup resulted in substantially higher H_2O_2 concentrations (290 μM vs. 1075 μM) and lower NO_3^- levels (4840 μM vs 1045 μM).

Plasma parameters for water treatment used in the study by Pandey et al. [69] were comparable to ours obtained for the *"Closed"* reactor (15 min, 25 ml, 11.2 W). The NO_2^- and NO_3^- concentrations were found to be 0.12 mM and 0.67 mM, respectively, therein. The concentration of nitrites is close to the one obtained in our study, but the concentration of nitrates is lower.

Furthermore, Xu et al. [70] used a DBD configuration for water

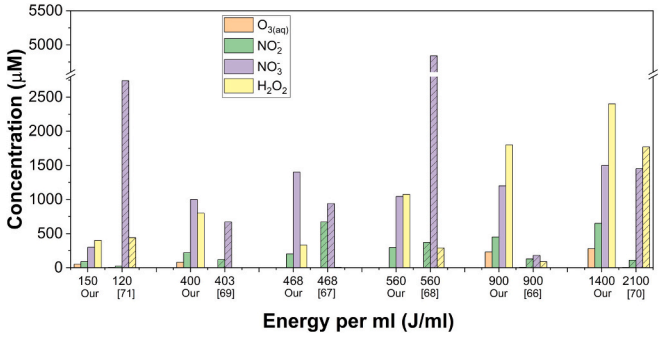

Fig. 15. Comparison of the liquid RONS concentrations in our work with the most relevant literature results. *"Our"* corresponds to the presented results that were obtained in the *"Open"* or *"Closed"* reactors while using tap water electrode.

treatment with a liquid volume of 10 ml and input power ranging from 22 to 35 W. The measured concentrations were 1.77 mM, 1.45 mM, 0.11 mM, and 4.2 μM for H_2O_2, NO_3^-, NO_2^-, and $O_{3(aq)}$, respectively. Notably, the concentrations of H_2O_2 and NO_3^- obtained in their study were in good agreement with our findings in the case of the *"Open"* reactor, even though we applied approximately half of their input power. However, the concentrations of ozone and nitrite in our study were significantly higher, suggesting distinct effects of our SDBD plasma in comparison to the standard DBD configurations.

In a study conducted by Kovacevic et al. [71], a falling film dielectric barrier discharge (DBD) reactor was employed to measure reactive species generated in various gases, including air, with an average power input of 60 W. The authors reported higher concentrations of reactive species when compared to our study, taking into account the input energy per milliliter. Specifically, in distilled water exposed to air, concentrations of H_2O_2 were reported at 440 μM, $O_{3(aq)}$ at 5 μM, NO_3^- at 2.74 mM, and the maximum concentration of NO_2^- was 22 μM corresponding to 120 J/ml.

As DBD can also be ignited using pulsed high voltage, it is worth noting several related studies.

In a study by Laurita et al. [72], a nanosecond pulsed DBD air plasma was employed to treat liquids with comparable volumes and treatment times as presented in our study. Nevertheless, the measured RONS concentrations were notably lower than ours, indicating potential differences in the plasma treatment dynamics or efficiency.

In another study by Lukes et al. [31] used a DBD plasma setup, treating larger volumes (900 ml) of aqueous solutions. However, the reported RONS concentrations in their case were considerably lower than those observed in our study. Notably, H_2O_2 was reported around 220 μM, while NO_2^- and NO_3^- concentrations were 100 μM and 150 μM, respectively.

The measured RONS concentrations in this study, compared to other studies summarized in Fig. 15, can be attributed to several factors: reactor geometry, electrode configuration, power input methods, and treatment conditions. The position of plasma reactors relative to the liquid surfaces, the chamber dimensions, and the gas flow conditions all significantly influence the plasma-liquid interactions and subsequent chemical processes resulting in liquid RONS.

For a broader perspective and a more comprehensive comparison of various plasma types and their respective effects on RONS generation in liquids, the reader is referred to the review by Montalbetti [73], which provides a detailed evaluation of a wide spectrum of plasma modalities and their relevance to aqueous-phase chemical processing.

5. Conclusion

In this study, we introduce and evaluate three distinct air plasma reactor designs of SDBD with a liquid electrode operating at a three-phase interface (plasma-solid-liquid). We systematically investigate the effects of the three designs on RONS generation in direct interaction with liquids, using two types of liquids (oxalic acid solution and tap water) selected for their different chemical properties and relevance to both fundamental studies and practical applications. All three systems enabled substantial transfer of plasma-generated species into the liquids.

One of the key findings is the variability in the formation of RONS despite the same input powers, which reveals the complex interaction between the reactor geometry and plasma-liquid chemistry and transport. A substantial drop in the pH of the liquid (tap water) also highlighted the influence of reactor geometry on plasma chemistry.

In the *"Open"* reactor, with unrestricted ambient air supply, we experienced a strong ozone generation in both gas and liquid, accompanied by hydrogen peroxide, nitrite, and nitrate ion production in both liquids, even in acidic oxalic acid solution.

On the other hand, the *"Closed"* reactor, with its limited air circulation conditions and high air relative humidity, experienced varied RONS concentration trends, including reduced ozone concentrations and variations in nitrite, while the highest nitrate concentrations in both liquids. This reactor provides the highest efficiency in nitrogen species retention in the liquid phase within the context of this study, making it a promising approach for applications where nitrogen fixation is desired.

The "*In-tube*" reactor displayed intermediate behavior, with ozone suppression similar to the "*Closed*" reactor but nitrate trends more closely aligned with the "*Open*" system.

The use of oxalic acid solution consistently performed better than tap water for RONS generation in all reactor geometries. This highlights the importance of the liquid selection in plasma applications: while tap water offers simplicity and accessibility, oxalic acid significantly enhanced the plasma intensity, the filament density, and the RONS production efficiency.

Taken together, these results demonstrate that the unique combination of the SDBD system with a liquid electrode can effectively generate and transfer a broad spectrum of RONS into liquids. By showing that altering the liquid phase composition and reactor confinement significantly modifies the chemical environment and thereby the reaction pathways and product profiles, this study provides experimentally grounded insight that is directly relevant for plasma-assisted material modification and functionalization.

CRediT authorship contribution statement

Oleksandr Galmiz: Writing – review & editing, Writing – original draft, Project administration, Methodology, Investigation, Funding acquisition, Formal analysis, Data curation, Conceptualization. **Richard Cimerman:** Writing – review & editing, Writing – original draft, Formal analysis, Data curation. **Zdenko Machala:** Writing – review & editing, Writing – original draft, Supervision, Project administration, Funding acquisition.

Declaration of Generative AI and AI-assisted technologies in the writing process

During the preparation of this work, the authors used ChatGPT in order to improve the language and readability of the text. After using this tool, the authors reviewed and edited the content as needed and take full responsibility for the content of the publication.

Funding sources

This work was funded by the EU NextGenerationEU through the Recovery and Resilience Plan for Slovakia under the project No. 09I03-03-V04-00094 and 09I03-03-V03-00033, and by Marie Skłodowska-Curie Action Postdoctoral Fellowship under Horizon Europe with grant agreement number 101066764.

Declaration of competing interest

The authors declare that they have no known competing financial interests or personal relationships that could have appeared to influence the work reported in this paper.

Acknowledgements

The authors gratefully acknowledge Large Research Infrastructure CEPLANT for the provision of high-voltage equipment, which significantly contributed to the realization of this research, as well as Assoc. Prof. Mario Janda for his cooperation and valuable scientific guidance.

Appendix A. Supplementary data

Supplementary data to this article can be found online at https://doi.org/10.1016/j.cej.2026.173630.

Data availability

Data will be made available on request.

References

[1] P.J. Bruggeman, M.J. Kushner, B.R. Locke, J.G.E. Gardeniers, W.G. Graham, D. B. Graves, R.C.H.M. Hofman-Caris, D. Maric, J.P. Reid, E. Ceriani, D. Fernandez Rivas, J.E. Foster, S.C. Garrick, Y. Gorbanev, S. Hamaguchi, F. Iza, H. Jablonowski, E. Klimova, J. Kolb, F. Krcma, P. Lukes, Z. Machala, I. Marinov, D. Mariotti, S. Mededovic Thagard, D. Minakata, E.C. Neyts, J. Pawlat, Z.L. Petrovic, R. Pflieger, S. Reuter, D.C. Schram, S. Schröter, M. Shiraiwa, B. Tarabová, P.A. Tsai, J.R.R. Verlet, T. von Woedtke, K.R. Wilson, K. Yasui, G. Zvereva, Plasma–liquid interactions: a review and roadmap, Plasma Sources Sci. Technol. 25 (2016) 053002, https://doi.org/10.1088/0963-0252/25/5/053002.

[2] K. Hsieh, H. Wang, B.R. Locke, Analysis of a gas-liquid film plasma reactor for organic compound oxidation, J. Hazard. Mater. 317 (2016) 188–197, https://doi.org/10.1016/J.JHAZMAT.2016.05.053.

[3] S. Mededovic Thagard, G.R. Stratton, F. Dai, C.L. Bellona, T.M. Holsen, D.G. Bohl, E. Paek, E.R.V. Dickenson, Plasma-based water treatment: development of a general mechanistic model to estimate the treatability of different types of contaminants*, J. Phys. D. Appl. Phys. 50 (2016) 014003, https://doi.org/10.1088/1361-6463/50/1/014003.

[4] T. Morishita, T. Ueno, G. Panomsuwan, J. Hieda, A. Yoshida, M.A. Bratescu, N. Saito, Fastest formation routes of nanocarbons in solution plasma processes, Sci. Rep. 6 (1) (2016) 1–13, https://doi.org/10.1038/srep36880.

[5] D. Mariotti, J. Patel, V. Švrček, P. Maguire, Plasma–liquid interactions at atmospheric pressure for nanomaterials synthesis and surface engineering, Plasma Process. Polym. 9 (2012) 1074–1085, https://doi.org/10.1002/PPAP.201200007.

[6] C. Wei, F. Zhang, Y. Hu, C. Feng, H. Wu, Ozonation in water treatment: the generation, basic properties of ozone and its practical application, Rev. Chem. Eng. 33 (2017) 49–89, https://doi.org/10.1515/REVCE-2016-0008.

[7] E.S.M. Mouele, J.O. Tijani, K.O. Badmus, O. Pereao, O. Babajide, O.O. Fatoba, C. Zhang, T. Shao, E. Sosnin, V. Tarasenko, K. Laatikainen, L.F. Petrik, A critical review on ozone and co-species, generation and reaction mechanisms in plasma induced by dielectric barrier discharge technologies for wastewater remediation, J. Environ. Chem. Eng. 9 (2021), https://doi.org/10.1016/j.jece.2021.105758.

[8] K.D. Weltmann, T. Von Woedtke, Plasma medicine - current state of research and medical application, Plasma Phys. Control. Fusion 59 (2017), https://doi.org/10.1088/0741-3335/59/1/014031.

[9] V.P. Mayookha, R. Pandiselvam, A. Kothakota, S. Padma Ishwarya, A. Chandra Khanashyam, N. Kutlu, E.J. Rifna, M. Kumar, P.S. Panesar, A.A. Abd El-Maksoud, Ozone and cold plasma: emerging oxidation technologies for inactivation of enzymes in fruits, vegetables, and fruit juices, Food Control 144 (2023), https://doi.org/10.1016/j.foodcont.2022.109399.

[10] P. Sundriyal, M. Pandey, S. Bhattacharya, Plasma-assisted surface alteration of industrial polymers for improved adhesive bonding, Int. J. Adhes. Adhes. 101 (2020) 102626, https://doi.org/10.1016/J.IJADHADH.2020.102626.

[11] U. Kogelschatz, Dielectric-barrier discharges: their history, discharge physics, and industrial applications, Plasma Chem. Plasma Process. 23 (2003) 1–46.

[12] H.-E. Wagner, R. Brandenburg, K.V. Kozlov, A. Sonnenfeld, P. Michel, J.F. Behnke, The barrier discharge: basic properties and applications to surface treatment, Vacuum 71 (2003) 417–436, https://doi.org/10.1016/S0042-207X(02)00765-0.

[13] P. Bruggeman, C. Leys, Non-thermal plasmas in and in contact with liquids, J. Phys. D. Appl. Phys. 42 (2009) 053001, https://doi.org/10.1088/0022-3727/42/5/053001.

[14] D.B. Graves, The emerging role of reactive oxygen and nitrogen species in redox biology and some implications for plasma applications to medicine and biology, J. Phys. D. Appl. Phys. 45 (2012), https://doi.org/10.1088/0022-3727/45/26/263001.

[15] A. Khlyustova, C. Labay, Z. Machala, M.P. Ginebra, C. Canal, Important parameters in plasma jets for the production of RONS in liquids for plasma medicine: a brief review, Front. Chem. Sci. Eng. 13 (2019) 238–252, https://doi.org/10.1007/S11705-019-1801-8/METRICS.

[16] M.E. Hassan, M. Janda, Z. Machala, Transport of gaseous hydrogen peroxide and ozone into bulk water vs. electrosprayed aerosol, Water 13 (2021) 182, https://doi.org/10.3390/W13020182.

[17] K. Kučerová, Z. Machala, K. Hensel, Transient Spark Discharge Generated in Various N2/O2 Gas Mixtures: Reactive Species in the Gas and Water and Their Antibacterial Effects, Plasma Chem. Plasma Process. 40 (2020) 749–773, https://doi.org/10.1007/s11090-020-10082-2.

[18] D. Pavliňák, O. Galmiz, M. Zemánek, M. Černák, Design and evaluation of plasma polymer deposition on hollow objects by electrical plasma generated from the liquid surface, Plasma Process. Polym. 15 (2018) 1–12, https://doi.org/10.1002/ppap.201700183.

[19] O. Galmiz, M. Zemánek, D. Pavliňák, M. Černák, Plasma treatment of polyethylene tubes in continuous regime using surface dielectric barrier discharge with water electrodes, J. Phys. D. Appl. Phys. 51 (2018), https://doi.org/10.1088/1361-6463/aabb49.

[20] O. Galmiz, D. Pavliňák, M. Zemánek, A. Brablec, M. Černák, Hydrophilization of outer and inner surfaces of Poly(vinyl chloride) tubes using surface dielectric barrier discharges generated in ambient air plasma, Plasma Process. Polym. 14 (2017) e1600220, https://doi.org/10.1002/ppap.201600220.

[21] D. Pavliňák, O. Galmiz, M. Zemánek, A. Brablec, J. Čech, M. Černák, Permanent hydrophilization of outer and inner surfaces of polytetrafluoroethylene tubes using ambient air plasma generated by surface dielectric barrier discharges, Appl. Phys. Lett. 105 (2014) 154102, https://doi.org/10.1063/1.4898134.

[22] O. Galmiz, R. Cimerman, P. Pareek, M. Janda, Z. Machala, Production of reactive species by using surface dielectric barrier discharge in direct contact with water, Plasma Sources Sci. Technol. 34 (2025), https://doi.org/10.1088/1361-6595/adb3cb.

[23] O. Galmiz, D. Pavlinak, M. Zemanek, A. Brablec, M. Cernak, Study of surface dielectric barrier discharge generated using liquid electrodes in different gases, J. Phys. D. Appl. Phys. 49 (2016) 065201, https://doi.org/10.1088/0022-3727/49/6/065201.

[24] N. Cvetanović, O. Galmiz, P. Synek, M. Zemánek, A. Brablec, T. Hoder, Electron density in surface barrier discharge emerging at argon/water interface: quantification for streamers and leaders, Plasma Sources Sci. Technol. 27 (2018), https://doi.org/10.1088/1361-6595/aaa578.

[25] M.A. Malik, C. Jiang, R. Heller, J. Lane, D. Hughes, K.H. Schoenbach, Ozone-free nitric oxide production using an atmospheric pressure surface discharge – A way to minimize nitrogen dioxide co-production, Chem. Eng. J. 283 (2016) 631–638, https://doi.org/10.1016/J.CEJ.2015.07.092.

[26] R. Cimerman, E. Matʼaš, M. Sárený, K. Hensel, Electrical and optical characterization of multi-hollow surface dielectric barrier discharge in configuration with the air-exposed electrode, Phys. Plasmas 29 (2022), https://doi.org/10.1063/5.0101496.

[27] M. Janda, K. Hensel, P. Tóth, M.E. Hassan, Z. Machala, The role of HNO2 in the generation of plasma-activated water by air transient spark discharge, Appl. Sci. 11 (2021) 7053, https://doi.org/10.3390/APP11157053.

[28] H. Bader, J. Hoigné, Determination of ozone in water by the indigo method, Water Res. 15 (1981) 449–456, https://doi.org/10.1016/0043-1354(81)90054-3.

[29] B. Tarabová, P. Lukeš, M. Janda, K. Hensel, L. Šikurová, Z. Machala, Specificity of detection methods of nitrites and ozone in aqueous solutions activated by air plasma, Plasma Process. Polym. 15 (2018), https://doi.org/10.1002/PPAP.201800030.

[30] Z. Machala, B. Tarabova, K. Hensel, E. Spetlikova, L. Sikurova, P. Lukes, Formation of ROS and RNS in Water Electro-Sprayed through Transient Spark Discharge in Air and their Bactericidal Effects, Plasma Process. Polym. 10 (2013) 649–659, https://doi.org/10.1002/PPAP.201200113.

[31] P. Lukes, E. Dolezalova, I. Sisrova, M. Clupek, Aqueous-phase chemistry and bactericidal effects from an air discharge plasma in contact with water: evidence for the formation of peroxynitrite through a pseudo-second-order post-discharge reaction of H2O 2 and HNO2, Plasma Sources Sci. Technol. 23 (2014), https://doi.org/10.1088/0963-0252/23/1/015019.

[32] G.M. Eisenberg, Colorimetric determination of hydrogen peroxide, Ind. Eng. Chem. Anal. Ed. 15 (1943) 327–328, https://doi.org/10.1021/I560117A011.

[33] P. Griess, Bemerkungen zu der Abhandlung der HH. Weselsky und Benedikt “Ueber einige Azoverbindungen”, Ber. Dtsch. Chem. Ges. 12 (1879) 426–428, https://doi.org/10.1002/CBER.187901201117.

[34] M.J. Moorcroft, J. Davis, R.G. Compton, Detection and determination of nitrate and nitrite: a review, Talanta 54 (2001) 785–803, https://doi.org/10.1016/S0039-9140(01)00323-X.

[35] V. Veronico, P. Favia, F. Fracassi, R. Gristina, E. Sardella, Validation of colorimetric assays for hydrogen peroxide, nitrate and nitrite ions in complex plasma-treated water solutions, Plasma Process. Polym. 18 (2021) 2100062, https://doi.org/10.1002/PPAP.202100062.

[36] H. Grosch, T. Hoder, K.D. Weltmann, R. Brandenburg, Spatio-temporal development of microdischarges in a surface barrier discharge arrangement in air at atmospheric pressure, Eur. Phys. J. D 60 (2010) 547–553, https://doi.org/10.1140/epjd/e2010-00239-8.

[37] J. Voráč, P. Synek, V. Procházka, T. Hoder, State-by-state emission spectra fitting for non-equilibrium plasmas: OH spectra of surface barrier discharge at argon/water interface, J. Phys. D. Appl. Phys. 50 (2017), https://doi.org/10.1088/1361-6463/aa7570.

[38] E. Moreau, C. Louste, G. Touchard, Electric wind induced by sliding discharge in air at atmospheric pressure, J. Electrost. 66 (2008) 107–114, https://doi.org/10.1016/j.elstat.2007.08.011.

[39] A. Dascalu, V. Pohoata, K. Shimizu, L. Sirghi, Molecular species generated by surface dielectric barrier discharge micro-plasma in small chambers enclosing atmospheric air and water samples, Plasma Chem. Plasma Process. 41 (2021) 389–408, https://doi.org/10.1007/s11090-020-10122-x.

[40] Z. Falkenstein, J.J. Coogan, Microdischarge behaviour in the silent discharge of nitrogen–oxygen and water–air mixtures, J.Phys.D:Appl.Phys 2 (1997) 817–825.

[41] X. Bian, Z. He, J. Zhu, X. Pi, S. Wan, L. Qi, Effects of humidity on variation of negative corona-generated space charge in rod to plane electrode, J. Eng. Des. 2019 (2019) 2869–2872, https://doi.org/10.1049/JOE.2018.8426.

[42] H. Ryzko, Drift velocity of electrons and ions in dry and humid air and in water vapour, Proc. Phys. Soc. 85 (1965) 1283, https://doi.org/10.1088/0370-1328/85/6/327.

[43] A.A. Abdelaziz, T. Ishijima, T. Seto, Humidity effects on surface dielectric barrier discharge for gaseous naphthalene decomposition, Phys. Plasmas 25 (2018), https://doi.org/10.1063/1.5020271/905284.

[44] I.A. Kossyi, A.Y. Kostinsky, A.A. Matveyev, V.P. Silakov, Kinetic scheme of the non-equilibrium discharge in nitrogen-oxygen mixtures, Plasma Sources Sci. Technol. 1 (1992) 207, https://doi.org/10.1088/0963-0252/1/3/011.

[45] W. Tian, M.J. Kushner, Atmospheric pressure dielectric barrier discharges interacting with liquid covered tissue, J. Phys. D. Appl. Phys. 47 (2014), https://doi.org/10.1088/0022-3727/47/16/165201.

[46] R. Cimerman, K. Hensel, Multi-hollow surface dielectric barrier discharge: production of gaseous species under various air flow rates and relative humidities, Plasma Chem. Plasma Process. 43 (2023) 1411–1433, https://doi.org/10.1007/s11090-023-10381-4.
[47] X. Zhang, B.J. Lee, H.G. Im, M.S. Cha, Ozone production with dielectric barrier discharge: effects of power source and humidity, IEEE Trans. Plasma Sci. 44 (2016) 2288–2296, https://doi.org/10.1109/TPS.2016.2601246.
[48] S. Jodzis, Application of technical kinetics for macroscopic analysis of ozone synthesis process, Ind. Eng. Chem. Res. 50 (2011) 6053–6060, https://doi.org/10.1021/IE102603Z.
[49] D. Braun, U. Kuchler, G. Pietsch, Behaviour of NOx in air-fed ozonizers, Pure Appl. Chem. 60 (1988) 741–746, https://doi.org/10.1351/PAC198860050741.
[50] T. Shimizu, Y. Sakiyama, D.B. Graves, J.L. Zimmermann, G.E. Morfill, The dynamics of ozone generation and mode transition in air surface micro-discharge plasma at atmospheric pressure, New J. Phys. 14 (2012) 103028, https://doi.org/10.1088/1367-2630/14/10/103028.
[51] B. Eliasson, U. Kogelschatz, Modeling and applications of silent discharge plasmas, IEEE Trans. Plasma Sci. 19 (1991) 309–323, https://doi.org/10.1109/27.106829.
[52] S. Park, W. Choe, C. Jo, Interplay among ozone and nitrogen oxides in air plasmas: Rapid change in plasma chemistry, Chem. Eng. J. 352 (2018) 1014–1021, https://doi.org/10.1016/J.CEJ.2018.07.039.
[53] J. Pawłat, P. Terebun, M. Kwiatkowski, B. Tarabová, Z. Kovaľová, K. Kučerová, Z. Machala, M. Janda, K. Hensel, Evaluation of oxidative species in gaseous and liquid phase generated by mini-gliding arc discharge, Plasma Chem. Plasma Process. 39 (2019) 627–642, https://doi.org/10.1007/S11090-019-09974-9.
[54] B. Eliasson, U. Kogelschatz, Nonequilibrium volume plasma chemical processing, IEEE Trans. Plasma Sci. 19 (1991) 1063–1077, https://doi.org/10.1109/27.125031.
[55] U. Kogelschatz, P. Baessler, Determination of nitrous oxide and dinitrogen pentoxide concentrations in the output of air-fed ozone generators of high power density, Ozone Sci. Eng. 9 (1987) 195–206, https://doi.org/10.1080/01919518708552335.
[56] A.A. Abdelaziz, T. Ishijima, T. Seto, N. Osawa, H. Wedaa, Y. Otani, Characterization of surface dielectric barrier discharge influenced by intermediate frequency for ozone production, Plasma Sources Sci. Technol. 25 (2016), https://doi.org/10.1088/0963-0252/25/3/035012.
[57] R. Peyrous, The effect of relative humidity on ozone production by corona discharge in oxygen or air – a numerical simulation – part II: air, Ozone Sci. Eng. 12 (1990) 41–64, https://doi.org/10.1080/01919519008552454.
[58] Z. Machala, B. Tarabová, D. Sersenová, M. Janda, K. Hensel, Chemical and antibacterial effects of plasma activated water: correlation with gaseous and aqueous reactive oxygen and nitrogen species, plasma sources and air flow conditions, J. Phys. D. Appl. Phys. 52 (2019), https://doi.org/10.1088/1361-6463/aae807.
[59] W.J. Weber, W. Stumm, Buffer systems of natural fresh waters, J. Chem. Eng. Data 8 (1963) 464–468, https://doi.org/10.1021/JE60018A062.
[60] G.B. Ndiffo Yemeli, R. Švubová, D. Kostolani, S. Kyzek, Z. Machala, The effect of water activated by nonthermal air plasma on the growth of farm plants: case of maize and barley, Plasma Process. Polym. 18 (2021), https://doi.org/10.1002/ppap.202000205.
[61] S. Kooshki, P. Pareek, M. Janda, Z. Machala, Selective reactive oxygen and nitrogen species production in plasma-activated water via dielectric barrier discharge reactor: an innovative method for tuning and its impact on dye degradation, J. Water Process Eng. 63 (2024) 105477, https://doi.org/10.1016/J.JWPE.2024.105477.
[62] Y. Gorbanev, C.C.W. Verlackt, S. Tinck, E. Tuenter, K. Foubert, P. Cos, A. Bogaerts, Combining experimental and modelling approaches to study the sources of reactive species induced in water by the COST RF plasma jet, Phys. Chem. Chem. Phys. 20 (2018) 2797–2808, https://doi.org/10.1039/C7CP07616A.
[63] S.P. Sander, R.R. Friedl, J. Abbatt, J.R. Barker, J.B. Burkholder, C.E. Kolb, M. J. Kurylo, G.K. Moortgat, P.H. Wine, R.E. Huie, V.L. Orkin, Chemical Kinetics and Photochemical Data for Use in Atmospheric Studies Evaluation Number 16. Supplement to Evaluation 15: Update of Key, 2010.
[64] J.L. Sotelo, F.J. Beltran, F.J. Benitez, J. Beltran-heredia, Henry's law constant for the ozone-water system, Water Res. 23 (10) (1989) 1239–1246.
[65] D.W. O'Sullivan, M. Lee, B.C. Noone, B.G. Heikes, Henry's law constant determinations for hydrogen peroxide, methyl hydroperoxide, hydroxymethyl hydroperoxide, ethyl hydroperoxide, and peroxyacetic acid, J. Phys. Chem. 100 (1996) 3241–3247, https://doi.org/10.1021/JP951168N.
[66] H. Xu, F. Zhu, Y. Liu, L. Quan, B. Li, H. Zhang, M. Shao, K. Xie, Effects of the ground-electrode temperature on the plasma physicochemical processes and biological inactivation functions involved in surface dielectric barrier discharge, Plasma Sources Sci. Technol. 31 (2022), https://doi.org/10.1088/1361-6595/ac9d63.
[67] R. Agus, L. Pipoz, F. Avino, A. Lavrikova, B. Myers, I. Furno, Plasma-activated water retains antimicrobial properties against Escherichia coli after 72 h of storage, Plasma Phys. Contr. Fusion 67 (2024) 015014, https://doi.org/10.1088/1361-6587/AD9950.
[68] P.R. Rotondo, D. Aceto, M. Ambrico, A.M. Stellacci, F. Faretra, R.M. De Miccolis Angelini, P.F. Ambrico, Physicochemical properties of plasma-activated water and associated antimicrobial activity against fungi and bacteria, Sci. Rep. 2025 15:1 15 (2025) 5536-. doi:https://doi.org/10.1038/s41598-025-88369-7.
[69] S. Pandey, R. Jangra, K. Ahlawat, R. Mishra, A. Mishra, S. Jangra, R. Prakash, Selective generation of nitrate and nitrite in plasma activated water and its physicochemical parameters analysis, Phys. Lett. Sect. A: Gen. Atom. Solid State Phys. 474 (2023), https://doi.org/10.1016/j.physleta.2023.128832.
[70] Z. Xu, X. Chen, X. Jin, S. Hu, Y. Lan, W. Xi, W. Han, C. Cheng, Study on the effective removal of chlorpyrifos from water by dielectric barrier discharge (DBD) plasma: the influence of reactive species and different water components, Chem. Eng. J. 473 (2023), https://doi.org/10.1016/j.cej.2023.144755.
[71] V.V. Kovačević, B.P. Dojčinović, M. Jović, G.M. Roglić, B.M. Obradović, M. M. Kuraica, Measurement of reactive species generated by dielectric barrier discharge in direct contact with water in different atmospheres, J. Phys. D. Appl. Phys. 50 (2017), https://doi.org/10.1088/1361-6463/aa5fde.
[72] R. Laurita, D. Barbieri, M. Gherardi, V. Colombo, P. Lukes, Chemical analysis of reactive species and antimicrobial activity of water treated by nanosecond pulsed DBD air plasma, Clin. Plasma Med. 3 (2015) 53–61, https://doi.org/10.1016/j.cpme.2015.10.001.
[73] R. Montalbetti, Z. Machala, M. Gherardi, R. Laurita, Production and chemical composition of plasma activated water: a systematic review and meta-analysis, Plasma Process. Polym. (2024), https://doi.org/10.1002/PPAP.202400249.